RSC Advances

PAPER

View Article Online
View Journal | View Issue

Cite this: *RSC Adv.*, 2021, **11**, 4210

Fabrication of a lead ion selective membrane based on a polycarbazole Sn(IV) arsenotungstate nanocomposite and its ion exchange membrane (IEM) kinetic studies†

Mohd. Zeeshan, *[a] Rais Ahmad,[a] Asif Ali Khan,*[a] Aftab Aslam Parwaz Khan,[bc] Guillermo C. Bazan,[d] Basma Ghaleb Alhogbi,[c] Hadi M. Marwani[bc] and Sakshi Singh[e]

A polycarbazole-Sn(IV) arsenotungstate (Pcz-SnAT) nanocomposite cation exchanger membrane (CEM) was prepared *via* the casting solution technique utilizing polycarbazole-Sn(IV) arsenotungstate and PVC (polyvinyl chloride) as a binder. The synthesis of the Pcz-SnAT membrane was confirmed *via* various characterization methods such as EDX, SEM, TGA, XRD, and FTIR spectroscopy. This membrane having a 4.5 : 1 composition ratio of composite by PVC exhibited the most effective outcomes for swelling, thickness, porosity, and water content. Our research indicates that the present ion selective membrane electrode is selective towards Pb(II) ions, with the detection limit ranging from 1×10^{-7} mol L^{-1} to 1×10^{-1} mol L^{-1} where 20 s is the response time and 3–7 is the working value pH. The mechanism of the Pcz SnAT ion exchange membrane was obtained by kinetic studies by utilizing the equation given by Nernst Planck at 40–80 °C. As a result, activation energy and thermodynamic studies were done. The analytical utility of this electrode is conventional by utilizing it as an electrode indicator within the potentiometric titration.

Received 2nd September 2020
Accepted 17th December 2020

DOI: 10.1039/d0ra07534e

rsc.li/rsc-advances

1 Introduction

Ion exchangers have been extensively utilized over the last few years for a variety of applications, primarily for the procedure of decontamination done chemically to recover metal ions, the regeneration of decontaminants, as well as for the removal of excess chemical formations occurring in the coolant.[1] Moreover, they find their applications simultaneously in power systems, semiconductors, softening processes, nuclear science, potable and ground water purification, sweeteners and sugar, pharmaceutical and petrochemical processing, chemicals, metal finishing, hydrometallurgy, beverages, food and other industries, potable water cleaning apparatus, nuclear industry microelectronics, recycling of industrial waste, food production, biotechnology, metal recovery and medicine.[2–15] In whole, ion exchange is an effective application in scientific investigation, chemical evaluation as well as for industrial specialists employed in the area of separating procedures.[16] In order to explore new properties by mixing inorganic materials with organic materials as ion exchangers, novel ion exchangers were developed *via* incorporating the acidic salts of multivalent metals in organic conducting polymers such as polyaniline, poly-*o*-toluidine, and poly-*o*-anisidine.[17–20] As a result, an 'organic–inorganic' nanocomposite cation exchanger was developed with enhanced granulometric as well as mechanical properties, better ion exchange capacity, higher stability of all kinds: mechanical, thermal and chemically good reproducibility with higher selectivity of heavy metals. All these qualities show that it is very helpful for environmental applications. A variety of inorganic-organic composite ion exchange materials were prepared in the lab and used successfully in making ISEs[21–25] and some of them[26–28] were used as selective electrodes for Pb(II) detection in the concentration range of 1×10^{-7} mol L^{-1}. to 1×10^{-1} mol L^{-1}. As a result of exposure to lead into both tap water as well as paint, the residual chemical in products of personal care and processed items of food, lead determination and detection in trace quantity still remains the topic of discussion by analytical chemistry or environmental science scientists. We have recently prepared CNT composites for an ion-selective membrane electrode and Pb sensor.[29,30] In

[a]*Department of Applied Chemistry, F/O Engineering and Technology, Aligarh Muslim University, Aligarh, 202002, India. E-mail: mohd.zee2010@gmail.com; asifalikhan2008@gmail.com*

[b]*Center of Excellence for Advanced Materials Research, King Abdulaziz University, Jeddah 21589, Saudi Arabia*

[c]*Chemistry Department, King Abdulaziz University, Jeddah-21589, Saudi Arabia*

[d]*Department of Materials and Chemistry & Biochemistry, University of California Santa Barbara, CA 93106,, USA*

[e]*Department of Chemistry, Amity School of Engineering and Technology, Amity University, Gwalior, Madhya Pradesh, India*

† Electronic supplementary information (ESI) available. See DOI: 10.1039/d0ra07534e

this study, the polycarbazole Sn(IV) arsenotungstate nanocomposite cation exchanger was synthesized and was discovered to be highly selective towards Pb(II) ions, with enhanced ion exchange capability. Various ion exchange studies and Pb(II) separation from some other large metal ions were done utilizing the exchanger. Polycarbazole-Sn(IV) arsenotungstate nanocomposite CEM had also been effectively employed for the separation of metallic ions.

2 Materials and methods

2.1 Chemicals, reagents and instruments

Carbazole for synthesis was obtained from HiMedia (HiMedia Laboratories Pvt. Ltd), and other chemicals used for the synthesis were as follows: ferric chloride (Merck, 98%), chloroform ($CHCl_3$) (Rankem), sodium arsenate, CDH (sodium tungstate), $SnCl_4 \cdot 5H_2O$ (CDH), orthophosphoric acid (H_3PO_4) (Qualigens, India), HCl (Merck India), and lead nitrate (Merck, India). All the chemicals and reagents were of analytical grade. Various instruments used basically for different characterizations were as follows: SEM, EDX was carried out by utilizing a Jeol JSM-6510 LV microscope, a BX-model Spectrum FTIR spectrophotometer (Perkin–Elmer, United States) in the 4000 to 400 nm range was used, thermo-gravimetric analysis was carried out using a 2.2A version 9900 DuPont, and XRD was performed on an X-ray powder diffractometer provided by Rigaku, with Cu Kα $\lambda = 1.54186$ Å, making use of a diffractometer based on 1148/89 working on PW using the radiation of Cu Kα. An Equiptronics EQ609 digital potentiometer having an accuracy $\pm$ 0.1 mV was utilized along with a calomel electrode.

2.2 Synthesis of the inorganic precipitate of Sn(IV) arsenotungstate

Sn(IV) arsenotungstate was obtained at 25 $\pm$ 2 °C ambient temperature by blending sodium chloride (0.1 mol L^{-1}), stannic chloride (0.1 mol L^{-1}), and sodium arsenate (0.1 mol L^{-1}) in a ratio of 1 : 1 : 1, respectively. After that, the solution was stirred constantly at the pH value of 1. Sn(IV) arsenotungstate (basically a white-colored gel) obtained was therefore allowed to settle down for about 24 h. Next, it was filtered and washed under given pH conditions. Lastly, in an oven, it was dried at 80 °C. Table S1† shows the various inorganic ion exchanger ratios. Due to higher IEC (ion exchange capability), test was chosen for further scientific researches.

2.3 Synthesis of the polycarbazole-Sn(IV) arsenotungstate (Pcz-SnAT) composite IEM

Sn(IV) arsenotungstate particles were used where Pcz-SnAT was obtained *via* the *in situ* substance oxidative polymerization method of polycarbazole. Then, Sn(IV) arsenotungstate (2 g) was taken in a 3-necked round bottom flask and dissolved in chloroform (250 mL), followed by stirring for about 30 min by utilizing a magnetic stirrer. After 30 min, a carbazole monomer of an appropriate amount was mixed and stirred further for 45 min for the carbazole adsorption on the arsenotungstate Sn(IV) particle surface area. In addition, an aqueous solution of $FeCl_3$ (formed by mixing $FeCl_3$ (2 g) with 250 mL chloroform) was mixed with the mixture and stirred further for 24 h. The green color of the solution indicates the formation of Pcz SnAT. For removing extra acid, the solution was filtered as well as washed using chloroform or methanol along with some $FeCl_3$ for removing any adhering trace residues. Lastly, final components were dried out at 50 °C in an oven, hence yielding the ion exchanger of the Pcz SnAT composite. According to different concentrations of the pyrrole monomer, different membranes labeled from P-1 to P-5 were synthesized, as shown in Table S2,† and their IEC was determined. Owing to its higher IEC, the Ppy-SnAT (P-4) sample was chosen for future studies.

2.4 Selectivity studies (K_d values)

The selectivity of the metal ions are largely based on a distribution behavior of the metal ion. During some practical applications, equilibrium is many handily conveyed in terminology of counter ions division coefficients. The K_d (distribution coefficient) value of different metallic ions on Pcz SnAT was obtained *via* the batch technique for different systems of solvents. In the H^+ ions, composite exchanger bead samples (100 mg L^{-1}) were taken in an Erlenmeyer flask having various metal nitrate solutions (20 mL) in the desired medium. These solutions were continuously stirred for 24 h. In a solution, the metal ion concentration before and after the experiment was found by titrating the solution against the EDTA solution (0.005 mol L^{-1}) (Table 1).[31] The ratio of concentration of metal ion ratio in a solution and the exchanger phase provides the distribution quantity, or in other words, the coefficient of distribution K_d in

Table 1 K_d values of metal ions on the Pcz-SnAT composite in different solvents

Solvents	HNO_3 in mol L^{-1}			H_2SO_4 in mol L^{-1}			HCl in mol L^{-1}			
Metal ions	0.1	0.01	0.001	0.1	0.01	0.001	0.1	0.01	0.001	DMW
Cu^{2+}	980	185	2190	1120	2260	1135	2015	830	910	1365
Ni^{2+}	415	425	285	1015	685	615	520	945	410	815
Pb^{2+}	1230	4925	4635	1595	2225	5015	4635	1785	1435	4015
Hg^{2+}	345	212	535	362	360	250	212	242	215	237
Ba^{2+}	915	1750	1210	1275	1005	1280	765	845	905	810
Cd^{2+}	875	585	905	985	510	635	695	395	485	535

a solution will be the way of measuring an uptake fractionally of metallic competing ions for the ions of H^+ using ion exchange materials as well as may certainly be mathematically estimated utilizing the formula:

$$K_d = (I - F)/F \times V/M \text{ (mL/g)} \quad (1)$$

Here, I is the number of moles of metal ion present initially in an aqueous phase, the solution (mL) volume is represented by V, the final amount of metal ions is represented by F in the aqueous phase, and the nanocomposite cation exchanger amount (g) is represented by M.

2.5 Preparation and characterization of the polycarbazole-Sn(IV) arsenotungstate (Pcz-SnAT) nanocomposite IEM

To prepare the ion-exchange membrane, Benson as well as Coetzee[32] processes were used to fabricate the electro-active Pcz-SnAT nanocomposite cation exchanger. The cation exchanger in different quantities were mixed in the powdered form, and after that they were analyzed for optimum membrane composition.[33] Next, they were carefully mixed with a proper amount of THF as well as PVC. The resulting solution was stirred for 48 h, and hence 4 membranes of various thicknesses, 0.23 mm, 0.19 mm, 0.15 mm, and 0.11 mm, were found. Table S3† provides the IEC membranes along with preparation conditions. Out of these, membrane M-3 was selected due to its excellent IEC.

In order to understand the orientation of the functional group, crystalline structure, thermal stability, elemental analysis, and surface morphology of the composite ion exchange membrane, a few important characterization techniques such as FTIR, XRD, TGA, EDX, SEM and EDX, were performed (Table S4†). Physicochemical characterization plays a significant role in understanding the functions of composite ion exchange membranes. Therefore, a few parameters, such as thickness, swelling, water content, and porosity, were found after applying composite ion exchange membrane conditions, as shown in Table 2. IEC membrane M-3 was chosen for future research due to its low thickness of about 0.11 mm.

2.6 Fabrication of the ion-selective membrane electrode

The sheet of the selected Pcz SnAT cation exchange membrane (0.11 mm thickness) as obtained through the process mentioned above was cut in the disc form and mounted on the lower end tubing of a Pyrex cup (o.d. 0.8 cm, i.d. 0.6 cm) with araldite. Lastly, the assembly was allowed to dry out under an air flow for 24 h. After that, the glass tube was filled with a 0.1 mol L^{-1} $Pb(NO_3)_2$ solution and kept at room temperature. A saturated calomel electrode was placed in the tubing for electric communication, and an additional saturated calomel electrode was utilized as the external reference electrode. The entire plan is shown as follows:

Internal "reference electrode" (SCE) (satd)	Internal electrolyte [0.1 mol L^{-1} Pb^{2+}]	Membrane	Sample solution	"External reference electrode" (SCE) (satd)

Different parameters, such as potentiometric titration, selectivity coefficient, working pH range, transport number, response time, electrode response curve, and low detection limit, were assessed to study the electrode.

2.7 Electrode response or membrane potential

The response of the electrode with the terminology with the terminology during 25 ± 2 °C of electrode potential, consequent to focus on the number of regular ways of 10^{-10} to 10^{-1} mol L^{-1}, $Pb(NO_3)_2$, has been found on continuous ionic strength according to the "IUPAC Commission for Analytical Nomenclature".[34] A plot of the electrode potential for the membrane *vs.* the ionic concentration was plotted using the electrode assembly. The graphs for the calibration were replicated thrice for checking the product reproducibility.

2.8 Transport number

The exchange membrane of Pcz-SnAT cation transport number of Pb(II) ions was estimated by utilizing eqn (2).

$$V_M = (2\bar{t}_{Pb(II)} - 1)RT/F \ln[C_2]/[C_1] \quad (2)$$

where V_M is the electrode potential of the membrane, $\bar{t}_{Pb(II)}$ is the transport number, C_2 is the higher concentration of the selected solution of Pb(II) and C_1 is the lower concentration of the selected solution of Pb(II).

2.9 pH effect

A series of solutions varying in pH levels of 1–10 have been ready at continuous concentration of ion which measures to be 1×10^{-1} mol L^{-1}. The pH value variations were because of the inclusion of dilute HCl acid as well as a solution of NaOH. The value of electrode at every pH value has been noted as well as plotted *versus* pH.

2.10 Response time

The response time was measured *via* recording an EMF for both the electrodes in terms of the time function if that has been

Table 2 Physiochemical characterization of Pcz-SnAT IEMs

Sample code	Thickness of the membrane (mm)	Porosity	Water content percentage weight of the wet membrane	Swelling
M1	0.19	0.0385	0.1925	0.041
M2	0.15	0.0605	0.2637	0.051
M3	0.11	0.0245	0.0917	0.019
M4	0.23	0.0435	0.3185	0.039

immersed in the under-analysis solution. In a bid to figure out the time of this experiment the following report was presented:

An electrode was initially dipped in a 1×10^{-1} mol L^{-1} ion concentrated solution and quickly shifted to the ion concentration of 1×10^{-2} mol L^{-1}. Zero second is the potential of the solution that simply means, in the second solution, electrode was dipped and consequently captured in a period of 5 s. A potential was then plotted *versus* time. The time period that all potentials achieved the frequent value symbolized the electrode's response period.

2.11 Titration studies

The analytical utility of this particular one electrode membrane was developed by using it in the form of a sign in a potentiometric titration electrode of the $Pb(NO_3)_2$ solution (0.01 mol L^{-1}) for the option of EDTA in titrant form. Possible values were plotted against the amount of EDTA utilized.

2.12 Selectivity coefficient

The response for the presence of the main ion along with the presence of additional foreign ions is calculated in terminology of the coefficient of potentiometric selectivity by utilizing mixed solution technique[35] (Table S5†). The coefficient of selectivity was estimated by utilizing the mentioned equation:

$$K_{AB}^{POT} = \frac{a_A}{(a_B)z_A/z_B} \quad (3)$$

where a_A and a_B are activities of primary and interfering ions with varying concentrations of primary ions and fixed concentration of interfering ions and ion charges are presented by z_A and z_B.

2.13 Chronopotentiometric studies

The selected Pcz-SnAT membrane electrode was dipped in a $Pb(NO_3)_2$ solution (1×10^{-1} mol L^{-1}) for 5, 10, 20, 30, 40, 50, and 60 s at 40 °C, 60 °C, and 80 °C with continuously mixing of the solution. The potential was noted as well as plotted against time at various temperatures.

3 Results and discussion

In situ polymerization was utilized to prepare the Pcz-SnAT composite ion exchange substances. The composite ion exchange had IEC for Na^+ identical to 2.5 meq g^{-1}, as shown in Table S2.† IEC is inversely proportional to the carbazole monomer. To examine the content potential in separating metallic ions, distribution studies for metallic ions were carried out *via* various solvent methods. Table 1 shows that the values of K_d are able to differ with the nature as well as structure of solvents. It was observed from the K_d-values in DMW along with other solvent methods that Pb^{2+} is clearly adsorbed whereas Cd^{2+}, Ni^{2+}, Cu^{2+}, Hg^{2+}, and Ba^{2+} indicate comparatively small surface area adsorption of composite ion exchange materials. An excessive uptake to specific metallic ions shows not just the qualities of ion exchange but additional ion selective attributes and the adsorption of the cation exchanger. A real difference in adsorption behaviour for various media would basically be defined by variations in the balance of metal exchange constants.

The variety of samples of Pcz-SnAT composite IEM were well prepared using 1000, 750, 500, and 250 mg L^{-1} contents with a fixed quantity of THF (25 mL) along with binder PVC (200 mg L^{-1}); the membrane was examined for thickness, cracks, materials distribution, surface uniformity, mechanical stability, and so on. The composite ion-exchange membranes of various ratio IEC for Na^+ were discovered as 0.62, 0.95, 0.37, and 0.48 meq g^{-1}. Preparation conditions along with IEC of the composite ion exchange membrane are provided in Table S3.†

Fig. 1 shows SEM images of Pcz-SnAT as well as Pb^{2+} absorbed Pcz-SnAT composite IEM under various magnifications. The polymeric "composite ion exchange membrane is porous in nature as well as forms thick membrane. Fig. 1(b)" exhibits a distinct absorption of Pb^{2+} in Pcz-SnAT membrane pores. The components contained in the Pcz-SnAT as well as after Pb^{2+} adsorption on the Pcz-SnAT composite ion exchange membrane were Pb, As, W, Sn, Cl, Fe, O, N, and C, and the portion structure of the components in the IEM are provided in Table S4† as well as confirmed from Fig. 2.

Fig. 3 shows the FTIR spectra of Pcz-SnAT and Pcz-SnAT dipped in the Pb(II) ion solution. In the spectra, the stretching frequency of –OH is observed at 3419 cm^{-1}, while the C–H stretching frequency is observed at 3050 cm^{-1} and 2927 cm^{-1};[36] the absorption peaks at 1603 cm^{-1} are attributed to the C=C stretching 1 of the quinoid rings and those at 1451 cm^{-1} are attributed to the C=C 1 stretching of the Pcz benzenoid ring. The peak at 1328 cm^{-1} is attributed to the C–N stretching mode, whereas the peak at 1005 cm^{-1} is attributed to the C–H out-of-plane bending vibration of 1,4 substituted benzenoid rings that confirmed the creation of Pcz. The FTIR spectra of Pcz-SnAT dipped in Pb(II) ion solution.

In this spectrum, the stretching frequency of –OH is shown at 3419 cm^{-1}, while the C–H stretching frequency is observed to be at 3050 cm^{-1} and 2927 cm^{-1}, as well as a broad band at 856 cm^{-1} and 1012 cm^{-1} having peak intensity at 928 cm^{-1} is because of the ionic phosphate group, while –O bonding is attributed to the 725 cm^{-1} peak value. At 1603 cm^{-1}, the absorption peaks are due to the C=C extending mode of the quinoid rings and the C=C stretching of polycarbazole benzenoid band was represented at peak 1452 cm^{-1}, which even

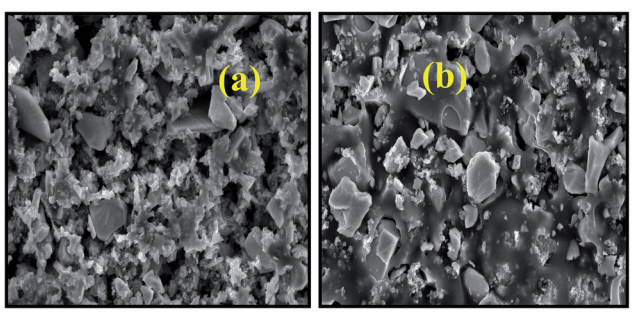

Fig. 1 The SEM images of (a) the Pcz-SnAT nanocomposite membrane and (b) adsorbed Pb(II) Pcz-SnAT nanocomposite membrane.

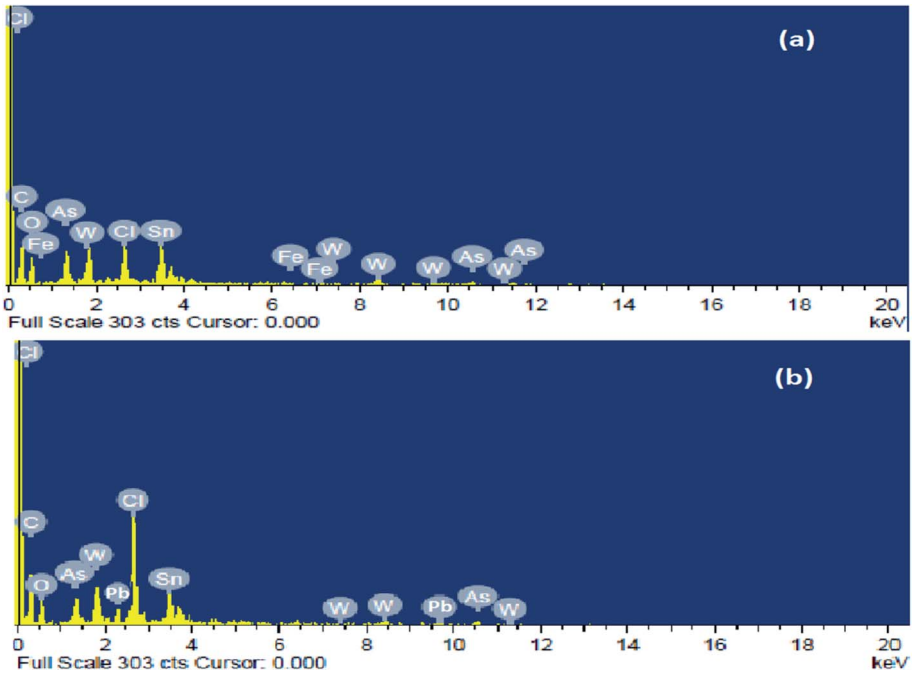

Fig. 2 EDX images of (a) the Pcz-SnAT nanocomposite membrane and (b) the adsorbed Pb(II) composite membrane.

suggests that the carbazole polymerization continues to be effectively attained on the surface area of the SnAT contaminants. The presence of $Pb(NO_3)$ in the dipped membrane is shown by 2 peak values of 1329 cm^{-1} and 2857 cm^{-1}. Peak assemblies at 856 to 441 cm^{-1} were moved to 802 to 437 cm^{-1}.[37] In Scheme 1, the formation of the Pcz-SnAT ion exchange membrane is shown due to results of EDX along with FTIR. In the scheme step I, $FeCl_3$ is used as an oxidant for oxidizing the carbazole monomer to a radical cation where one electron is removed from the radical cation in an oxidative-aromatization reaction for the formation of a carbazole dimer because in dimer conjugation is more as compared to monomer. Therefore it is more easily oxidized than the carbazole monomer and cation was oxidized immediately as well as further it also proceeds for polymerization reaction till each and every monomer are utilized. Hence, polycarbazole was produced. In an aqueous solution of $FeCl_3$ after the polycarbazole got oxidized in step 2, step 3 was used where polycarbazole binds to the Sn(IV) arsenotungstate matrix. In Scheme 2, the IEM that was adsorbed onto the lead metal ion intermingled with Pcz-SnAT for the formation of Pcz-SnAT IEM adsorbed in Pb(II).

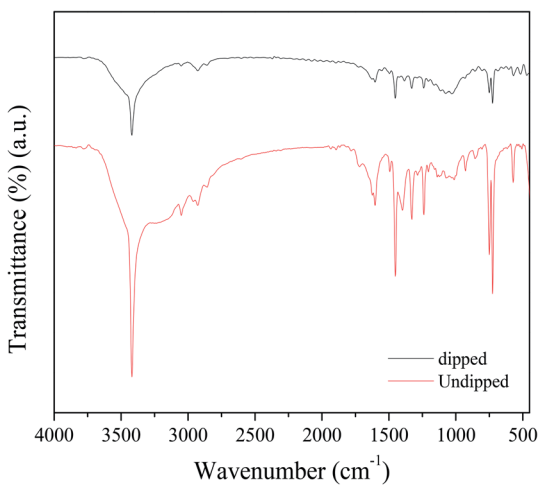

Fig. 3 FTIR spectra of Pb(II) dipped and undipped nanocomposite.

In Fig. 4, various weight losses are shown in the TGA curves. In the Pcz SnAT ion exchange membrane, ~5% weight-loss up to 200 °C is shown by the TGA curve that might be because of the elimination of water molecules; also, at 300 °C ~47% decomposition of the membrane is shown, whereas at 550 °C easy weight reduction of ~23% is observed, and at 650 °C, an additional weight loss of ~28% is noticed. TGA results show very clearly that at 650 °C Pcz-SnAT IEM is thermally stable. In Pb(II)-adsorbed Pcz-SnAT IEM, a weight-loss of ~5% up to 200 °C is shown by the TGA curve that might be because of the elimination of water molecules; also, at 300 °C, ~53% decomposition of the membrane is observed, whereas at 500 °C an easy weight reduction of ~5% was observed, and at 650 °C, an additional weight loss of ~22% was observed.

It can be seen in the TGA graph that at 650 °C Pb(II) adsorbed Pcz-SnAT IEM. XRD of Pcz SnAT as well as adsorbed Pb(II) of Pcz SnAT IEM was performed using the Rigaku X-ray powdered diffractometer with Cu anode (Kα $\lambda = 1.54186$ Å) in the range of $20° \leq 2\theta \leq 80°$ at 30 kV. The XRD pattern of the on-exchange membrane is shown in Fig. 5 at ambient temperature. It can be clearly found from the Pcz-SnAT XRD pattern (as prepared) that the ion exchange membrane is present in an amorphous form since there is no sharp peak in the pattern, and the Pb(II) adsorbed Pcz-SnAT IEM shows a peak at 25° that indicates the

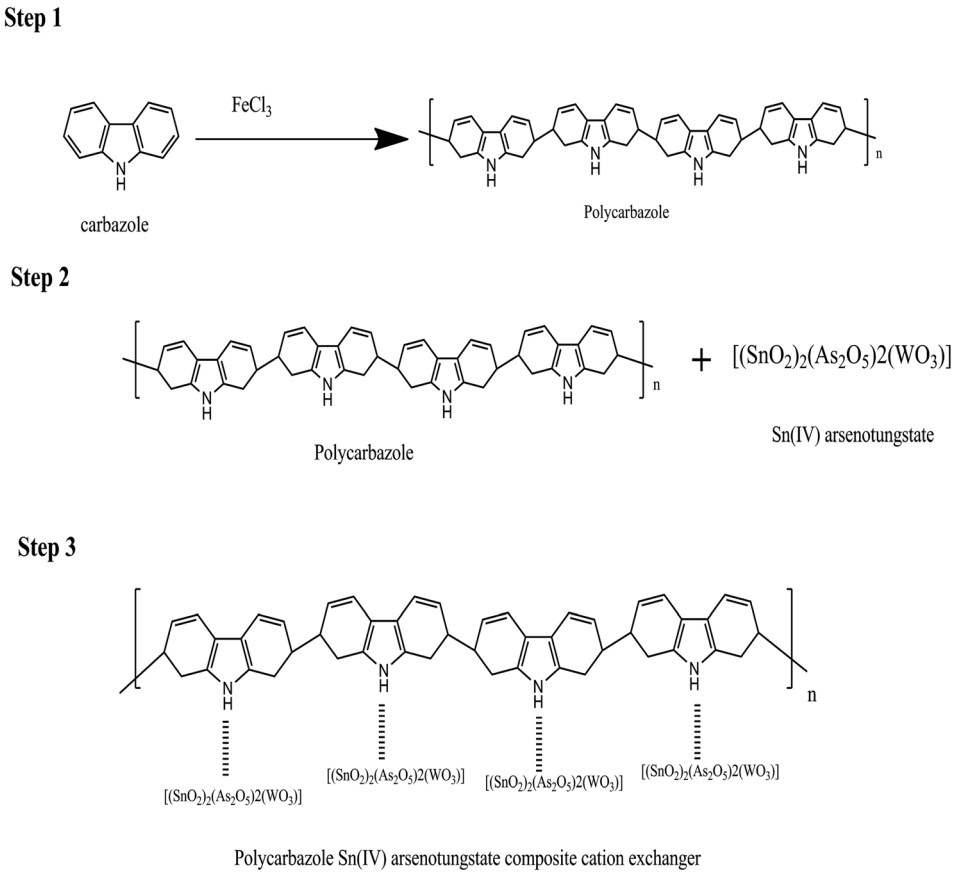

Scheme 1 The graphic illustration for the preparation of Pcz-SnAT IEM.

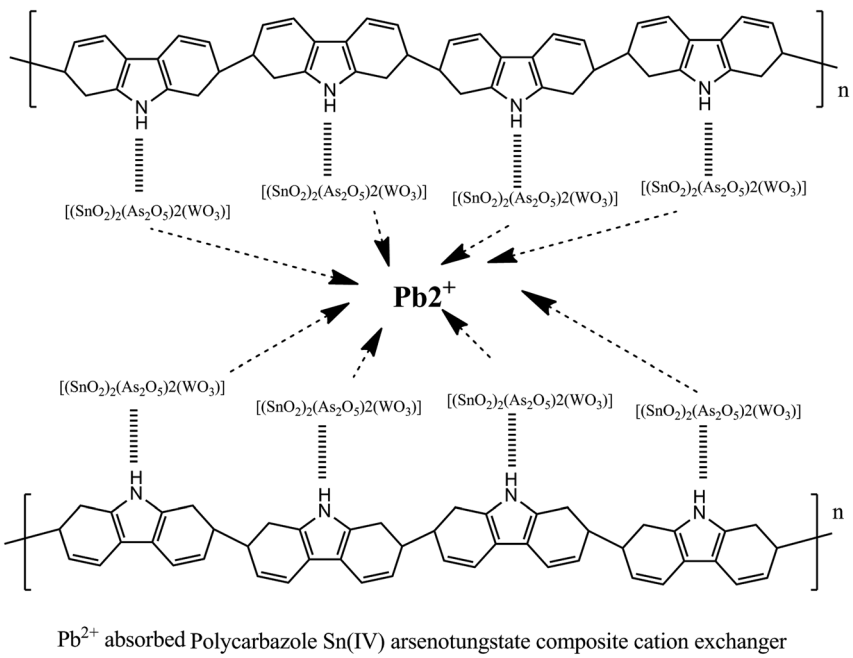

Scheme 2 The schematic of the formation of Pcz-SnAT IEM interactions with Pb^{2+}.

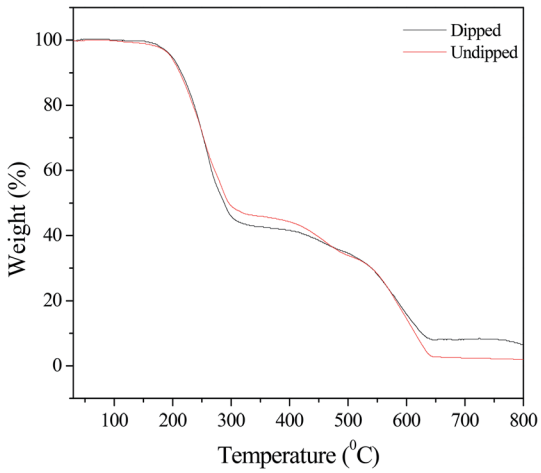

Fig. 4 TGA photographs of the Pcz-SnAT nanocomposite membrane and Pb(II)-adsorbed composite membrane.

presence of Pb(II) ions.[38] Physicochemical characterizations of Pcz-SnAT IEM were also important to make an ISE. Therefore, few properties, such as water content capability, porosity, thickness, and swelling, are listed in Table 2. An electrode based on ion was made by utilizing Pcz-SnAT IEM that has 0.23, 0.11, 0.15, and 0.19 mm thickness. Hence, less thickness of porosity, swelling and water content implies that interstices are negligible as well as diffusion throughout the membranes would exist primarily throughout the exchanger location.

Due to low thickness, IEC membrane M-3 along with porosity was selected for future research work. In addition, using small quantities of Sn(IV) arsenotungstate in polycarbazole Sn(IV) arsenotungstate has been demonstrated to be a superior strategy to enhance the qualities of Pcz-SnAT IEM. The composite statically maintained its mechanical and thermal stability excellently, although, the IEC permselectivity of the membranes were enhanced. When Sn(IV) arsenotungstate was added with the organic polymer (polycarbazole), the

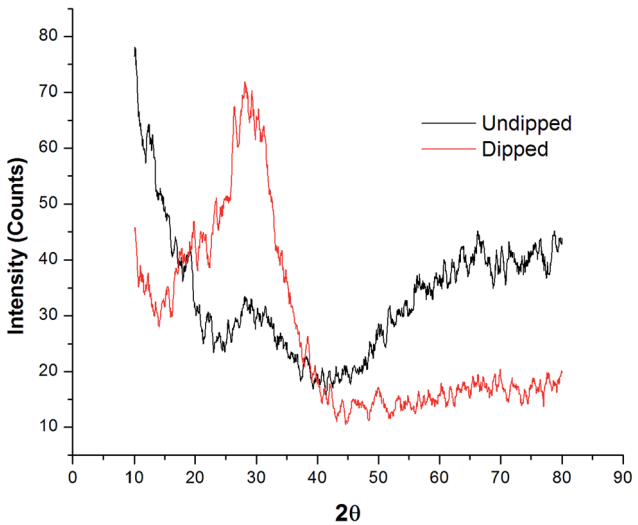

Fig. 5 XRD spectra of Pb(II) dipped and undipped nanocomposites.

porosity of the membranes was improved through the particle cluster formation. For ionic species toward successfully pass through that are extremely useful qualities because of "the ion exchange membranes particularly the transportation phenomena as well as permeability of the membranes that are because of the porosity and pore measurements of the" membranes. In order to enhance the transport phenomena and the IEC composite ion exchange membrane, pore distribution along with the pore size plays an essential part. Selectivity and sensitivity of an ion-selective electrode are basically dependent on the behavior of electro-active material.

If membrane of these materials were placed among these 2 electrolyte solutions with same characteristics, but at various metallic (picky membrane is) ion concentrations, the ion exchange diffusion occurs; the lead ion selective membrane had been replaced with the H^+ ions present on the membrane surface area, therefore creating an electric potential distinction, that is, a potential membrane. Fig. S1† shows various concentrations ranging from 1×10^{-10} mol L^{-1} to 1×10^{-1} mol L^{-1} of the Pcz-SnAT IEM electrode (M-4). The electrode exhibits a linear result in the range of 1×10^{-7} mol L^{-1} to 1×10^{-1} mol L^{-1} having 22.92 mV value Nerstian slope per decade alteration in concentration.

The detection limit was found from the intersection of the extrapolated sections of the calibration graph,[39–41] and for the Pcz-SnAT ion exchange membrane, it was discovered as 1×10^{-9} mol L^{-1}. Therefore, for Pb(II), the concentration of membrane (M-4) was obtained in the range from 1×10^{-7} mol L^{-1} to 1×10^{-1} mol L^{-1}. In Fig. S2† the transportation quantity *vs.* concentration has also been determined for good understanding with electrode having the 1×10^{-7} mol L^{-1} to 1×10^{-1} mol L^{-1} concentration range. The potential response of the electrode was the calculated Pb(II) ions concentration in different pH values at 1×10^{-2} M. It was obvious that the electrode potential is still the same in the pH range of 3.0–7.0.

The Fig. S3† recognized the pH electrode assortment. Time response plays a vital part in ISE and the obtained average time is described as the time required for the electrode to reach a stable potential after the successive immersion of the electrode in different ion solutions, each having a 10-fold difference in concentration.

Fig. S4† shows the results of the Pb(II) ion solution response time. As mentioned in the figure, ~20 s is the membrane response time. This synthesized membrane might be used up to six weeks with no important change in prospect where the potential slop is reproducible for ±1 mV per concentration. In a potential when a drift was noticed, a membrane was equilibrated again having 0.1 mol L^{-1} $Pb(NO_3)_2$ solution for 3 to 4 days.

Owing to the good selectivity of the Pb(II) selective electrode, this is used as a indicator electrode for the titration of Pb(II) against an EDTA solution as titrant. The EDTA addition causes a decrease in prospective corresponding to the decrease in free metal ion concentration that is Pb(II) because of the complexation of its with EDTA Fig. S5.†

In a solution, the quantity of Pb(II) might be correctly decided out of the ensuing assembled titration curve giving an equivalent sharp stage. This analysis started where the practical usage of a recommended exchanger of composite cation in membrane electrode. The selectivity behavior is driven if the

solid measurement of the goal test was achievable or perhaps not. It was determined by MSM (mixed solution method) and also observed in Table S5† that majority of the ions that interfered proved to have lower coefficient values of selectivity which indicated that absolutely interference in an assembly of membrane electrode as well as its functionality. This amazing Pb(II) selectivity more than additional ions mirrors an excessive membrane affinity for Pb(II).

3.1 Kinetics of ion exchange

The kinetic measurements of the Pb^{2+}–H^+ membrane were done under given favorable conditions for the phenomenon of ion-exchange diffusion-controlled particles. The particle diffusion-controlled occurrence is preferred by particle size as well as the concentration of materials contained inside a membrane. Diffusion of the film is crucial in a few devices that clearly shows more concentration of the fixed ionic set of the membrane.

The results were very impressive with regards to the attainment of fractional equilibrium $U(\tau)$, as per the following (4) equation.

$$U(\tau) = \frac{\text{The amount of exchanger at time '}t\text{'}}{\text{The amount of exchanger at infinite time}} \quad (4)$$

Plots of $U(\tau)$ *versus* t (min) Pb^{2+} in Fig. 6 indicated that for achieving equilibrium fractionally became more pronounced in temperature of high level, which showed increased Pb^{2+} mobility with increased temperature. Each value of $U(\tau)$ decrease in the uptake was also noticed with time.

The numerical results can be expressed based on the Nernst–Planck equation through explicit approximation.[42,43]

$$U(\tau) = \{1 - \exp[\pi^2(f_1(\alpha)\tau + f_2(\alpha)\tau^2 + f_3(\alpha)\tau^3)]\}^{1/2} \quad (5)$$

where τ is the half time of exchange $= \bar{D}_{H^+} t/r_0^2$, α is the mobility ratio $= \bar{D}_{H^+}/\bar{D}_{Pb(II)}$, r_0 is the membrane radius, and $\bar{D}_{H^+}$ and $\bar{D}_{Pb(II)}$ are the inter diffusion coefficients of counter ions H^+ and Pb^{2+}, respectively, in the exchanger membrane phase. The functions $f_1(\alpha)$, $f_2(\alpha)$ and $f_3(\alpha)$ are governed by the mobility ratio (α) and the charge ratio ($\bar{Z}_{H^+}/\bar{Z}_{Pb(II)}$) of the exchanging ions, and hence are expressed differently. When the membrane was taken in the H^+ form, and the substituting ion was lead for $1 \leq \propto \leq 20$, as in the present case, the three functions are given as:

$$f_1(\alpha) = -\frac{1}{0.64 + 0.36\alpha^{0.668}} \quad (6)$$

$$f_2(\alpha) = -\frac{1}{0.96 + 2.0\alpha^{0.4635}} \quad (7)$$

$$f_3(\alpha) = -\frac{1}{0.27 + 0.09\alpha^{1.140}} \quad (8)$$

The value of each $U(\tau)$ will have a consistent value of τ, which is obtained from the MATLAB software. Fig. 7 shows the plots against τ *versus* time at three different temperatures and obtained the linearity graph, confirming the Pb^{2+}–H^+ membrane diffusion control phenomenon.

3.2 Activation energy and thermodynamic studies

The S values from the slopes of several plots τ *versus* time are shown in Table S6.† The value S is related to equation as follows:

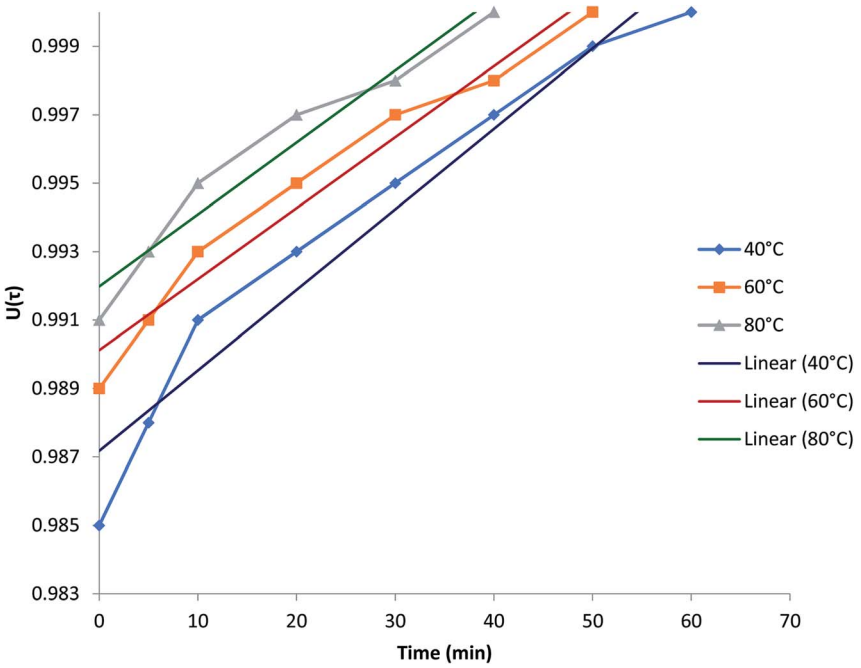

Fig. 6 Plots of $U(\tau)$ *versus* t (time) for Pb(II)–H^+ exchanges at different temperatures: 40 °C, 60 °C and 80 °C of the Pcz-SnAT composite IEM electrode.

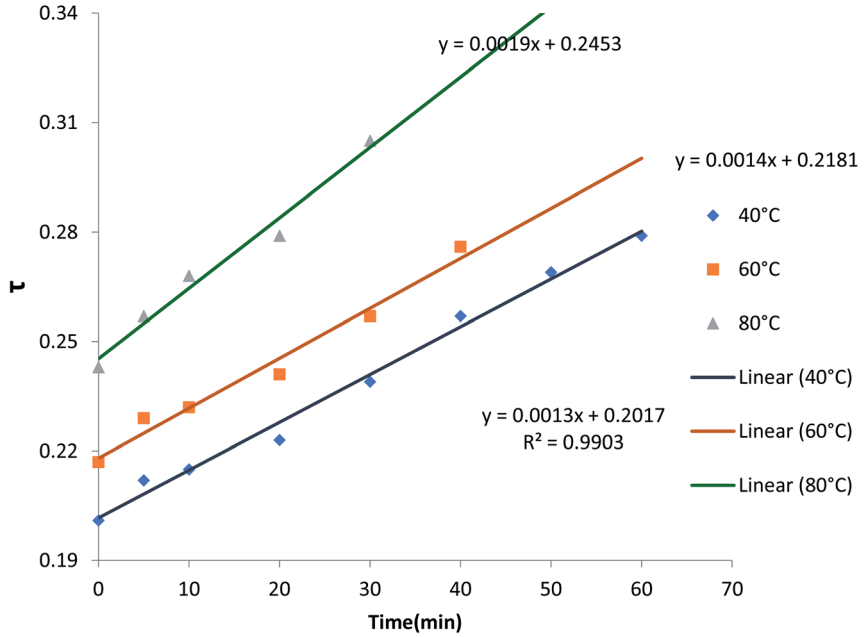

Fig. 7 Plots of τ *versus* t (time) for Pb(II)–H^+ exchanges at different temperatures: 40 °C, 60 °C and 80 °C on the PPYZP composite IEM electrode.

$$S = \bar{D}_{H^+}/{r_0}^2 \quad (9)$$

The values of $-\log \bar{D}_{H^+}$ obtained values by using eqn (9) graphed against $1000/T$ (K). A linearity line acquired confirming the Arrhenius equation validity;

$$-\log \bar{D}_{H^+} = D_0 \exp(-E_a/RT) \quad (10)$$

D_0 is obtained by extrapolating these lines and using the intercepts at the origin. Eqn (10) is used to calculate the E_a, the value of D_{H^+} putting at 273 K. The calculated ΔS° was by replacing value of D_0,

$$D_0 = 2.72d^2(kT/\hbar)\exp(\Delta S^\circ/R) \quad (11)$$

where d is the ionic jump distance taken as 5 Å, k is the Boltzmann constant, R is the gas constant, $\hbar$ is Plank's constant and T is taken as 273 K.

The values of D_0, E_a, ΔS° and ΔG° thus obtained are briefed in Table S7.†

ΔH° of the ion exchange reaction was done using the following equation

$$\Delta H^\circ = E_a - nRT \quad (12)$$

ΔG° corresponding to room temperature was calculated using the following equation.[44]

$$\Delta G^\circ = \Delta H^\circ - T\Delta S^\circ \quad (13)$$

It is obvious from the ion exchange examined that the accomplishment of equilibrium was quicker at higher temperatures. This can be explained by the fact that the diffusion rate is higher *via* the thermally amplified points of the matrix of ion exchange. The plots of τ *versus* time show the film diffusion phenomena, as in Fig. 7. Table S7† depicts that a lower activation energy (E_a) prefers faster metal ions during the exchange. Positive values of the entropy change (ΔS°) and negative values of free energy of activation (ΔG°) show that reactions of ion exchange are spontaneous and easily possible at the surface of the cat IEM.

4 Conclusions

In this current research work, the Pcz-SnAT composite cat IEM was synthesized and characterized *via* XRD, TGA, FTIR, EDX, and SEM for their morphological and chemical analyses. In addition, the formulated Pcz-SnAT composite membrane was found to have a 0.95 meq g^{-1} IEC. Such an exchange membrane of composite ions was used in the form of an electroactive component to produce ion-selective membrane electrodes in aqueous solutions as well as to determine Pb(II). The membrane electrode showed the detection limit ranging from 1×10^{-7} mol L^{-1} to 1×10^{-1} mol L^{-1}, where 20 s is the response time and 3–7 is the working pH range. The mechanism of ion exchange studies recommends that the controlled-diffused film ion exchange as well as with the outcomes of substantial parameters such as low E_a (activation energy) mainly prefer metal ion to change positive as well as fast values of ΔS° (change in entropy) shows the ion exchange reactions are basically feasible as well as spontaneous on the Pcz-SnAT membrane surface.

Abbreviations

ISE	Ion selective electrode
CEM	Cation exchange membrane

Pcz-SnAT	Polycarbazole-Sn(IV)arsenotungstate
SEM	Scanning electron microscopy
EDX	Energy dispersive X-ray analysis
FTIR	Fourier transform infra-red spectroscopy
TGA	Thermogravimetric analysis
XRD	X-Ray diffraction analysis
IEC	Ion exchange capability
IEM	Ion exchange membrane
K_d	Distribution coefficient
EDTA	Ethylene diaminetetracetic acid
THF	Tetrahydrofuran
PVC	Polyvinyl chloride
EMF	Electromotive force
DMW	Demineralized water
MSM	Mixed solution method

Conflicts of interest

There are no conflicts to declare.

Acknowledgements

The project was funded by the Deanship of Scientific Research (DSR), King Abdulaziz University, under grant no. 22-130-36-HiCi. The authors, therefore, acknowledge with thanks DSR technical and financial support.

References

1 H. Li and L. Zou, Ion-exchange membrane capacitive deionization: a new strategy for brackish water desalination, *Desalination*, 2011, **275**, 62–66.
2 W. Du, X. Liu, R. Tian, R. Li, W. Ding and H. Li, Specific ion effects of incomplete ion-exchange by electric field-induced ion polarization, *RSC Adv.*, 2020, **10**, 15190–15198.
3 S. Imaizumi, H. Matsumoto, M. Ashizawa and T. A. Minagawa, Nanosize effects of sulfonated carbon nanofiber fabrics for high capacity ion-exchanger, *RSC Adv.*, 2012, **2**, 3109–3114.
4 A. Mautner, H. A. Maples, H. Sehaqui, T. Zimmermann, U. P. d Larraya, A. P. Mathew, C. Y. Lai, K. Lif and A. Bismarck, Nitrate removal from water using a nanopaper ion-exchanger, *Environ. Sci.: Water Res. Technol.*, 2016, **2**, 117–124.
5 H. Dong, L. Wei and W. H. Tarpeh, Electro-assisted regeneration of pH-sensitive ion exchangers for sustainable phosphate removal and recovery, *Water Res.*, 2020, **184**, 116167.
6 M. A. Khan, Fabrication and applications of polyaniline Zr(IV)iodate nanocomposite ion exchanger for heavy metal sorption with antibacterial activity, *Groundw. Sustain. Dev.*, 2020, **11**, 100427.
7 A. A. Zagorodni, *Ion Exchange Materials Properties and Applications*, Elseiver, Oxford, UK, 1st edition, 2007.
8 I. Kusumoto, Medium optimization by combination of response surface methodology and desirability function: an application in glutamine production, *J. Nutr.*, 2001, **131**, 2552–2555.
9 J. D. Sherman, Synthetic zeolites and other microporous oxide molecular sieves, *Proc Nat Acad Sci Jpn*, 1999, 3471–3478.
10 J. A. Dale and J. A. Greig, in *Ion exchange at the millennium London*. Imperical College Press, 2000 pp. 261–8.
11 K. Das, M. Anis, B. M. N. M. Azemi and N. Ismail, Fermentation and recovery of glutamic acid from palm waste hydrolysate by ion-exchange resin column, *Biotechnol. Bioeng.*, 1995, **48**, 551–555.
12 E. V. Calle, J. Ruales, M. Dornier, J. Sandeaux, R. Sandeaux and G. Pourcelly, Deacidification of the clarified passion fruit juice, *Desalination*, 2002, **149**, 357–361.
13 E. Vera, Comparison between different ion exchange resins for the deacidification of passion fruit juice, *J. Food Eng.*, 2003, **59**, 361–367.
14 S. E. Kentish and G. W. Stevens, Innovations in separations technology for recycling and reuse of liquid waste streams, *Chem. Eng. J.*, 2001, **84**, 149–159.
15 T. Nakanishi, N. Higuchi, M. Nomura, M. Aida and Y. Fujii, Nitrogen isotope separation with displacement chromatography using cryptand polymer, *J. Nucl. Sci. Technol.*, 1996, **33**, 341–345.
16 R. Harjula, J. Lehto, A. Paajanen, L. Brodkin and E. Tusa, Adsorption of strontium from acids solutions using an inorganic exchanger - uranium antimonite, *Nucl. Sci. Eng.*, 2001, **137**, 206–214.
17 C. V. Subban and A. J. Gadgil, Electrically regenerated ion-exchange technology for desalination of low-salinity water sources, *Desalination*, 2019, **465**, 38–43.
18 M. S. Malik, A. A. Qaiser and M. A. Arifa, Structural and electrochemical studies of heterogeneous ion exchange membranes based on polyaniline-coated cation exchange resin particles, *RSC Adv.*, 2016, **6**, 115046–115054.
19 A. A. Zagorodni, *Ion exchange materials: properties and applications*, Elsevier, Amsterdam, 2006.
20 A. A. Khan, L. Paquiza and A. Khan, An advanced nano-composite cation-exchanger polypyrrole zirconium titanium phosphate as a Th(IV)-selective potentiometric sensor: preparation, characterization and its analytical application, *J. Mater. Sci.*, 2010, **45**, 3610–3625.
21 A. A. Khan, A. Khan and Inamuddin, Preparation and characterization of a new organic–inorganic nano-composite Poly-o-toluidine Th(IV) phosphate: Its analytical applications as cation-exchanger and in making ion-selective electrode, *Talanta*, 2007, **72**, 699–710.
22 A. A. Khan, U. Habiba and A. Khan, Synthesis and characterization of organic– inorganic nanocomposite Poly-o-anisidine Sn(IV) arsenophosphate: its analytical applications as Pb(II) ion-selective membrane electrode, *Int. J. Anal. Chem.*, 2009, 659215.
23 Y. Shao, Y. Ying and J. Ping, Recent advances in solid-contact ion-selective electrodes: functional materials, transduction mechanisms, and development trends, *Chem. Soc. Rev.*, 2020, **49**, 4405–4465.

24 A. A. Khan and S. Shaheen, Determination of arsenate in water by anion selective membrane electrode using polyurethane-silica gel fibrous anion exchanger composite, *J. Hazard. Mater.*, 2014, **264**, 84.

25 A. A. Khan, S. Shaheen and U. Habiba, Synthesis and characterization of poly-o-anisidine Sn(IV) tungstate: A new and novel 'organic–inorganic' nano-composite material and its electro-analytical applications as Hg (II) ion-selective membrane electrode, *J. Adv. Res.*, 2012, **3**, 269.

26 A. A. Khan and S. Shaheen, Synthesis and characterization of a novel hybrid nano composite cation exchanger poly-o-toluidine Sn(IV) tungstate: Its analytical applications as ion-selective electrode, *Solid State Sci.*, 2013, **16**, 158.

27 A. A. Khan and S. Shaheen, Preparation, characterization of polyacrylonitrile–aluminum hydroxide composite anion exchanger and its analytical application as AsO_4^{-3} selective membrane electrode, *Composites, Part B*, 2014, **58**, 312.

28 A. A. Khan and S. Shaheen, Chronopotentiometric and electroanalytical studies of Ni(II) selective polyaniline Zr(IV) molybdophosphate ion exchange membrane electrode, *J. Electroanal. Chem.*, 2014, **714–715**, 38.

29 A. Khan, A. A. P. Khan, A. M. AsiriM, M. Rahman and B. G. Alhogbi, Preparation and properties of novel sol-gel-derived quaternized poly(n-methyl pyrrole)/Sn(II)SiO3/CNT composites, *J. Solid State Electrochem.*, 2015, **19**, 1479–1489.

30 A. A. P. Khan, A. Khan, M. M. Rahman, A. M. Asiri and M. Oves, Lead Sensors Development and Antimicrobial Activities Based on Graphene Oxide/Carbon Nanotube/Poly (OToluidine) Nanocomposite, *Int. J. Biol. Macromol.*, 2016, **89**, 198–205.

31 A. A. Khan, U. Habiba and A. Khan, Synthesis and Characterization of Organic-Inorganic Nanocomposite Poly-o-anisidine Sn(IV) Arsenophosphate: Its Analytical Applications as Pb(II) Ion-Selective Membrane electrode, *Int. J. Anal. Chem.*, 2009, **10**, 659215.

32 A. A. Khan, Inamuddin and M. M. Alam, Determination and separation of Pb2+ from aqueous solutions using a fibrous type organic–inorganic hybrid cation-exchange material: Polypyrrole thorium(IV) phosphate, *React. Funct. Polym.*, 2005, **63**, 119.

33 A. A. Khan, Inamuddin and M. M. Alam, Preparation, characterization and analytical applications of a new and novel electrically conducting fibrous type polymeric–inorganic composite material: polypyrrole Th(IV) phosphate used as a cation-exchanger and Pb(II) ion-selective membrane electrode, *Mater. Res. Bull.*, 2005, **40**, 289.

34 C. N. Reilley, R. W. Schmidt and F. S. Sadek, Chelon approach to analysis (I) survey of theory and application, *J. Chem. Educ.*, 1959, **36**, 555–564.

35 C. J. Coetzee and A. J. Benson, A cesium-sensitive electrode, *Anal. Chim. Acta*, 1971, **57**, 478–480.

36 A. Craggs, G. J. Moody and J. D. R. Thomas, PVC matrix membrane ion-selective electrodes Construction and laboratory experiments, *J. Chem. Educ.*, 1974, 51541.

37 G. G. Guilbault, Recommendation for publishing manuscripts on ion-selectiveelectrodes Commission on analytical nomenclature, analytical chemistrydivision, *Ion-Sel. Electrode Rev.*, 1969, **1**, 139.

38 Y. Umezawa, K. Umezawa and H. Sato, Selectivity coefficients for ion-selective electrodes: Recommended methods for reporting $K_{A,B}^{pot}$ values (Technical Report), *Pure Appl. Chem.*, 1995, **67**, 507.

39 A. A. Khan and S. Shaheen, Preparations and characterizations of poly-otoluidine/multiwalled carbon nanotubes/Sn(IV) tungstate composite ion exchange thin films and their application as a Pb(II) selective electrode, *RSC Adv.*, 2014, **4**, 23456.

40 A. A. Khan and S. Shaheen, Synthesis and characterization of a novel hybrid nano composite cation exchanger poly-o-toluidine Sn(IV) tungstate: Its analytical applications as ion-selective Electrode, *Solid State Sci.*, 2013, **16**, 158.

41 M. K. Amini, M. Mazloum and A. A. Ensaf, Lead selective membrane electrode using cryptand(222) neutral carrier Fresenius, *J. Anal. Chem.*, 1999, **364**, 690–693.

42 F. Helfferich and M. S. Plesset, Ion Exchange Kinetics A Nonlinear Diffusion Problem, *J. Chem. Phys.*, 1958, **28**, 424.

43 M. S. Plesset, F. Helfferich and J. N. Franklin, Ion Exchange Kinetics A Nonlinear Diffusion Problem II Particle Diffusion Controlled Exchange of Univalent and Bivalent Ions, *J. Chem. Phys.*, 1958, **29**, 1064.

44 K. G. Varshaney and A. A. Khan. *Proceedings of Indian science academy, Part A, Physical sciences*, India, 1990.